RSC Advances

ROYAL SOCIETY OF CHEMISTRY

www.rsc.org/advances

RSC Advances

ARTICLE

A direct synthesis of Si-nanowires on a 3D porous graphene as high performance anode material for Li-ion batteries

Received 00th January 20xx,
Accepted 00th January 20xx

DOI: 10.1039/x0xx00000x

www.rsc.org/

Fethullah Güneş [a]

Silicon nanowires (SiNWs) have been successfully synthesized on a three-dimensional porous graphene foam (GF) via chemical vapor deposition (CVD). The unique porous nanoarchitecture of three-dimensional graphene network enhances the electrical conductivity and provides improved Si-mass loadings. The obtained GF/SiNWs composite, with Si mass loadings of >0.3 mg.cm^{-2} shows high gravimetric and areal capacities, as well as comparable cycle life as an anode material in Li-ion battery. Alumina coating (ALD) of SiNWs also improved the cycle life and rate capability. This facile direct synthesis method of 3D porous architecture of GF/SiNWs composite demonstrates a new approach to improve the electrochemical performances of Si-based anode materials for Li-ion batteries.

Introduction:

The rapid development of modern society requires energy storage devices with a high energy/power density, long cyclic life and also miniaturization. Rechargeable Li-ion batteries (LIBs) have drawn great attention due to their potential applications in plug-in hybrid electric vehicles, portable electronics as well as integrated microsystems[1-8]. Among all kinds of different anode materials, silicon (Si) has become one of the most promising candidates owing to its high lithium storage capacity of 3572 mAh.g^{-1} at room temperature[9]. Yet, dramatic volume change during lithiation/delithiation processes causes electrical disconnection from current collectors and hence capacity fading, which is making this material impractical[10, 11]. Recently, tremendous efforts have been made to overcome this issue through: i) preparation of nanoscale Si structure, such as zero dimensional solid/hollow nanoparticles[12] and one dimensional nanowires/nanotubes (NWs/NTs)[13, 14], ii) Fabrication of Si-containing composite materials[15-20]. Although a significant progress was achieved with nanoscale Si structure, the use of additional binder and conductive additives usually increases the dead mass and thus reduce the capacity of the electrode[21-23]. In the case of Si-containing composite anode, carbon with a reasonable Li-insertion capacity (372 mAh.g^{-1})[23] has been widely used as an active matrix not only because of their good conductivity but also for their high elasticity which can be used as a stress buffering material for Si. For instance, carbon nanotube networks which can spare the use of binder were utilized as matrix materials showing improved capacity retentions compared to bare Si electrode[24, 25]. Porous carbon can hold Si particles in its 3D conducting matrix, and also provides space for expanded Si particles (after intercalation) by accommodating them within its porous framework. In both

[a] Department of Materials Science and Engineering, Faculty of Engineering and Architecture, Izmir Katip Celebi University, Cigli-Izmir, 35620 Turkey. E-mail: fethullah.gunes@ikc.edu.tr (Fethullah Güneş)

cases the matrix holds onto the Si-particles and hence preserves the electrical continuity within all Si particles. However, composite fabrication process can rather be complicated because of unrefined production methods, purifications, stable dispersion and further post-treatment processes. [26-28]. Graphene, a two-dimensional material along with good conductivity was also widely used as a matrix for Si-containing composite anode[29-33]. Compared to chemically derived graphene whose conductivity is rather low due to the existence of surface functional groups and high contact resistances between discontinued graphene flakes, graphene obtained by chemical vapour deposition (CVD) shows the highest conductivity, together with good electron mobility and high thermal conductivity[34]. Most noteworthy, graphene foam (GF) obtained by template-assisted CVD delivered a high electrical conductivity of 10 $S.cm^{-1}$ [35] and exhibited a unique three-dimensional (3D) interconnected porous structure. This special structure provides not only larger surface area for better access of electrolyte, but also faster electron transport and shorter ion diffusion length with respect to 2D graphene networks[36-38].

In this report, Si nanowires (SiNWs) were directly grown on Ni-foam template-assisted grown 3D porous graphene network. A high Si loading mass was achieved without using any binders or additives. This composite was tested as an anode material in LIB. Unique structure of this 3D composite provides an excellent access of electrolyte to SiNWs and compensate Si low conductivity with graphene's superior conductivity while accommodating large surface area for acceptable Si mass loading along with GF's strain relaxing elasticity resulting in high areal and gravimetric capacities and a reasonable cycle life.

Results and discussion

Fig.2 shows scanning electron microscopy (SEM) and transmission electron microscopy (TEM) images of graphene layers on Ni-foam (Fig.2a,), GF after Ni removal (Fig.2b), after SiNWs synthesis on GF (Fig.2c), and individual SiNWs (Fig.2d, 2e, 2f). Graphene layers synthesized on Ni-foam with different number of layers are continuous all over the foam (Fig.2a), enabling us to obtain interconnected 3D-GF with a little shrinkage after the removal of supporting Ni-foam (Fig.2b). After the SiNWs synthesis, GF is still intact, keeping the 3D foam structure, SiNWs are grown on outer surface of graphene layers and at even deep parts, thanks to large pores enabling precursors to reach in lower portions of the GF on SS during PE-CVD synthesis. (Fig.2c). Fig.2d and Fig.2f show an individual SiNW grown on GF with crystalline-Si (c-Si) core, amorphous-Si (a-Si) and 10 nm ALD coating shells. The upper inset of Fig.2d shows selected area electron diffraction (SAED) pattern of a SiNW which is consistent with the calculated-FFT pattern in the upper inset of Fig.2e. High resolution TEM image of an individual SiNW's crystal core is shown in Fig.2e, representing a single-crystal structure with 3.3 Å of lattice spacing.

For structural analyses of GF/SiNWs composite, X-ray diffraction spectroscopy (XRD) and Raman spectroscopy were performed as shown in Fig.3. The XRD spectrum (Fig.3a) of GF/SiNWs composite contains 6 perfectly distinguishable peaks associated with graphene at 26.6˚, 43.5˚ and 54.7˚; with Si at 28.5˚ and 47.3˚; and with Au (deposited as SiNW catalyst) at 38.2˚, which are consistent with the literature[39, 40]. The graphene peak at 43.5˚ may also be correlated to SS substrate as indicated in the Fig.3a. Raman spectroscopy of

GF/SiNWs composite (Fig.3b) shows a clear peak at ~ 517 cm^{-1}. In the case of c-Si, first order transverse-optical (TO) phonon mode will display a sharp peak at 520 cm^{-1} which usually becomes broaden and is downshifted when the long-range order in Si is lost[41]. In our case, a red shift of 3 cm^{-1} and a small broaden band at around 490 cm^{-1} are caused by the co-existence of c-Si and a-Si which is in good agreement of Fig.2. Fig.3c shows raman spectroscopy results from graphene foam as synthesized and sonicated in ethanol solution then as coated on Si/SiO_2 substrate. In some position on graphene flakes coated on Si/SiO_2 substrate obtained from graphene foam shows monolayer with very high intensity ratios of 2D/G bands as well as few layers in other positions with no observable D- peaks showing the high crystallinity of graphene foams with different number of graphitic layers.

Fig.4a shows the 2nd-cycle cyclic voltammograms (CV) of GF and GF/SiNWs composites with/without ALD coating. In the case of GF (black), charge peaks at 0.01 and 0.17 V (vs. Li/Li+) and discharge peaks at 0.2 and 0.27 V (vs. Li/Li+). The charge current associated with Li-Si alloying reaction in GF/SiNWs composite was observed at 0.01 and 0.2V (vs. Li/Li+) in the case of as prepared samples (red). Similarly in the case of ALD coated composite (blue), lithiation peaks were observed at 0.05 and 0.24 V (vs. Li/Li+) with a slight peak-shift which might be correlated to sluggish Li-Si reaction after ALD coating. In discharge state, for the GF/SiNWs composites, two peaks around 0.3 V and 0.5 V were observed as delithiation of Li-Si alloys and correlated to the discharge plateau at 0.4 V in the voltage profile curves (Fig.4a). These obtained results are in agreement with those for Si anodes [11] and for Si/Graphene composites[18, 42]. In the following cycles the magnitude of all current peaks were increased with cycling. Although CV profiles of ALD coated GF/SiNWs composite and uncoated one exhibit similar characteristics, the amplitude of ALD-coated sample is slightly smaller, indicating that insulating nature of alumina may affect the reaction of Si with Lithium ions, decreasing overall capacity slightly, at initial cycles.

Nyquist plots GF/SiNWs composites in Fig.4b, compares the as-prepared and ALD coated composites. Semicircle and the linear portions of the plots are indicating the electrode reactions are controlled by charge transfer at high frequencies and by diffusion at low frequencies. However, in the case of ALD-coated composite (before cycling), the second semicircle indicates that ALD-coating may slow down the diffusion at low frequencies initially, while showing a better diffusion for the later cycles with alumina's well known Li-permeable structure.[43] After 100 cycles of lithiation/delithiation, the charge resistance of both samples were increased, however, this increment was much smaller in the case of ALD-coated composites compared to that of as-prepared composites. This behavior can be attributed to that composite with ALD coating has better cycling stability, although they have slower charge transfer at the beginning, having a larger diameter of semi-circle before cycling. This results are in agreement with the results obtained by Wu Q H , et al.[8] and Ren J G, et al.[44] confirming the positive effect of ALD coating resulting in a stable battery performance and good electrochemical impedance characteristics[8, 44].

In Fig.5a and 5b, the voltage profiles of GF/SiNWs composites as prepared and with ALD-coating were shown, respectively. For the first cycles at a current density of 200 $mA.g^{-1}$, both samples show similar gravimetric discharge capacities of 2423 and 2494 $mAh.g^{-1}$. However, in following cycles at current density of 500 $mA.g^{-1}$, as-prepared composites showed faster decay in discharge capacity compared to that of ALD coated composite. For instance at 20th

cycle, ALD coated sample showed 83% capacity retention (2074 mAh.g^{-1}) while, as prepared sample retained only 76% of the first cycle. At 50th cycles, discharge capacities were decreased to 1125 mAh.g^{-1} and 875 mAh.g^{-1} for ALD coated and as-prepared samples, respectively. A flat plateau around 0.4 V (Li/Li+) was diminished at subsequent cycles as reported for the amorphization of Si to react with Li [11]. However, by ALD-coating this delayed reduction resulted in a comparably better cycling stability. Capacity-cycling profiles of the same samples in Fig.5a and Fig.5b was also shown in Fig.5c. For comparison, the calculated specific capacity of SiNWs from the same composite of GF/SiNW-ALD and pure SiNWs grown on stainless-steel (SS) substrate was added in Fig.5c. This SiNWs-only capacity from the composite with ALD-coating was calculated from the following equation[45]:

$$Q_{Si} = m_{GF}/m_{Si} \{Q_{composite} (1+ m_{Si}/m_{GF}) - Q_{GF}\}$$

where; "$Q_{composite}$" is the total capacity of GF/SiNWs composite, Q_{Si} and Q_{GF} are the specific capacities of SiNWs (only) and GF (only) per unit mass of each material and m_{Si} and m_{GF} are the mass of SiNWs and GF in the composite, respectively. As we know the specific capacity of GF-only and GF/SiNWs composite, we can obtain the specific capacity of "SiNWs-only" in the composite. Calculated SiNWs discharge capacity was ~3488 mAh.g^{-1} at first cycle (with 200 mA.g^{-1} current density) and decreased to 3480 mAh.g^{-1} in the second cycle and to 2545 mAh.g^{-1} at 25th cycle. Between 25th and 35th cycles, SiNWs showed a fast decay and at subsequent cycles a slower decay. In the case of "SiNWs on SS" in Fig.5c showed 2582 mAh.g^{-1} and 3302 mAh.g^{-1} charge and discharge capacity in the first cycle (with 200 mA.g^{-1} current density), respectively. In the following cycles (with 500 mA.g^{-1} current density), the pure SiNWs on SS showed a very fast decay and at 50th cycle decreased down to 525 and 538 mAh.g^{-1} charge and discharge capacities, respectively. As it can be observed from the plot, ALD-coated composites showed comparably better cycling stability than that of as-prepared GF/SiNWs composite and the pure SiNWs on SS. Coulombic efficiencies of the samples are shown in Fig.6. The first cycles of all samples showed very low first charge (lithiation) capacity, yet higher discharge (delithiation) capacity.. Reason for this is still unclear to us, however it might be due to polishing the Li foils by sand-paper before using to remove surface oxide, causing formation of fine Li-powder on the surface of Li-metal and these Li-particles may lithiate the highly porous graphene-foam during 24 h wetting time before cycling causing this phenomena. Therefore, for clarity Coulombic efficiencies of the first cycles were not shown for the composite samples. ALD-coating did not cause a noticeable change in Coulombic efficiencies of GF/SiNWs composites. In the second cycles, Coulombic efficiencies of GF-only, pure SiNWs on SS and GF/SiNWs composites were ~82%, 89%, and ~97%, respectively. GF/SiNWs composites' efficiencies then increased in third cycle to ~98%. GF-only sample was increased to 92% in third and kept increasing gradually to 99% at 100th cycle. SiNWs on SS sample was increased to 91% in third and kept increasing gradually until 97.5 at 50th cycle. In subsequent cycles up to 26th cycle, GF/SiNWs composites decreased to ~94% then gradually increased again up to ~98% at 100th cycle.

For investigating the rate capability of ALD-coated GF/SiNWs composites, different current densities of 200 mA.g^{-1}, 500 mA.g^{-1}, 1000 mA.g^{-1}, 2000 mA.g^{-1} and 4000 mA.g^{-1} were applied (Fig.5d). GF/SiNWs composites with ALD-coating showed stable and reversible capacities at high rates, such as ~850 mAh.g^{-1} and ~550 mAh.g^{-1} with current densities of 2000 and 4000 mA.g^{-1}, respectively, which are comparable to report for Si/carbon material

composites[46]. In Fig.7a, the areal capacities of GF/SiNWs composite and calculated capacities for only SiNWs were compared. Well-known large surface areas up to 850 $m^2.g^{-1}$ of GFs accommodate high mass loading of SiNWs over 0.3 $mg.cm^{-2}$. This unique high density Si mass loading improved the areal discharge capacities up to 1.8 $mAh.cm^{-2}$ for SiNWs-only and 1.3 $mAh.cm^{-2}$ for GF/SiNWs composite. Even after 100 cycles, discharge capacities of 0.5 $mAh.cm^{-2}$ for SiNWs-only and 0.35 $mAh.cm^{-2}$ for GF/SiNWs composite were achieved. The effect of ALD coating of alumina (ALD) for SiNWs-only can be seen in Fig.7b. Although, at initial cycles both ALD-coated and as-prepared samples show similar values, after 50 cycles, ALD-coated sample retained 45% of its original areal discharge capacity, while as-prepared sample retained only 36% of its original areal discharge capacity. High and low magnification SEM images taken after 100 cycles of ALD-coated GF/SiNWs composite confirmed that, although SEI-layer covered all over the surface, SiNWs in the composite were still observable. (Fig.8)

Experimental

Preparation steps of GF/SiNWs composite were depicted in Fig.1 GFs were synthesized on nickel foams (Alantum Advanced Technology Materials, China) with 420 g.m-2 in areal density and 1.6 mm in thickness by atmospheric pressure CVD. Nickel foams were placed in the center of a quartz tube of atmospheric pressure CVD chamber and samples were kept under Ar (500 sccm) and H_2 (200 sccm) at 1000 ˚C for reduction of surface oxide on Ni foams. CH_4 (3 sccm) was then flowed for 5 min with same amount of Ar and H_2. Following the synthesis, CH_4 was turned off and the chamber was cooled down to room temperature under the same Ar and H_2 ambient at a cooling rate of ≈100 ˚C.min^{-1}. Graphene coated Ni foams were then coated with poly (methyl methacrylate) (PMMA) solution and baked at 180 ˚C for 30 min followed by etching in Ni etchant (Transene Inc, TFB) at 90 ˚C for 5 h. After complete removal of Ni, GFs coated with PMMA were immersed into hot acetone for 30 min and transferred onto stainless steel (SS) substrates. For further details see ref [47] and [35] For the complete removal of PMMA, samples then annealed at 600˚C in ultrahigh vacuum chamber for 2 h. For the SiNWs growth on GF, samples were then deposited ~25 nm Au by e-beam evaporator, and placed into a plasma enhanced CVD (PECVD) chamber (A-Tech, South Korea). Samples in the chamber were heated up to 420˚C in H_2 (120 sccm) ambient followed by SiH_4 (30 sccm) introduction with plasma (RF power: 20 W) under pressure of 600 mTorr for 2h. After the synthesis of SiNWs, samples were cooled down to room temperature under vacuum (10^{-6} Torr). Before and after GF transfer, after Si deposition, each sample was carefully weighed, using an A&D microbalance BM-22 (A&D Company Limited, Japan) with a sensitivity and precision of 1 µg. Alumina (Al_2O_3) coating of SiNWs on GF was performed by an ALD system (Lucida D100, NCD Technology, Korea) at 200 ˚C using trimethyl aluminum (TMA) and H_2O as precursors. ALD film thickness was controlled by precursor pulse cycles where each cycle was fixed to 1Å per cycle. For all samples with ALD, 100 cycles were used to obtain 10 nm of ALD coating.

Scanning electron microscopy (JEOL, FESEM JSM-7600F) and high-resolution transmission electron microscopy (HR-TEM) (JEOL, JEM 2100F) were used to investigate the surface morphology and electron diffraction patterns of SiNWs. Raman spectroscopy (Renishaw, RM-1000 Invia) with excitation

energy of 2.41 eV (514 nm, Ar+ ion laser) was used to characterize the optical properties of the GF and SiNWs. X-ray diffraction (XRD) ((Bruker D2 Phaser) with CuKα radiation) patterns were used to analyze the crystal structure of GF/SiNWs composite.

Electrochemical properties were evaluated by galvonastatic cycling of coin cells (CR 2032) with GF/SiNWs composite on SS substrate as the working electrode and lithium foil (99.9% purity, 0.38 mm thickness, Sigma Aldrich) as the counter/reference electrode. The mass loading was 0.5~0.55 mg.cm^{-2} of composite with ~70 wt% mass loadings of SiNWs. The electrolyte for all tests was 1M LiPF6 in ethylene carbonate/diethyl carbonate (1:1 v/v, Puriel, Techno semichem Co. Ltd, Korea) and separators from (Celgard 2500) were used. After the assembly of coin cells in dry room, all cells were kept for 24 h as wetting time of samples in electrolyte. For all measurements the total mass of GF/SiNWs composite were used. Si-only specific capacities were calculated from capacities GF-only and GF/SiNWs composite specific capacities as explained in ref [45].

Conclusions

A facile direct fabrication route to the synthesis of SiNWs on a highly conductive porous 3D graphene network of GFs, with improved Si-mass loadings have been demonstrated. GF underneath the SiNWs utilized as a conductive and a flexible support to enhance the gravimetric and areal capacities at reasonable current densities. Furthermore, GF's excellent elastic property improved the stress induced pulverization of SiNWs, resulting in a better cycling performance of GF/SiNWs composite, though cycling performance still need to be improved. ALD coating of composite further comparably improved the cycle life. We believe this direct Si and 3D-graphene hybrid fabrication method can open up new possibilities for more advanced anode materials in Li-ion batteries.

Acknowledgement:

Special thanks to Prof. Young Hee Lee of Center for Integrated Nanostructure Physics IBS, Sungkyunkwan University for his valuable discussions and supports.

References:

1. L. Hu, H. Wu, Y. Gao, A. Cao, H. Li, J. McDough, X. Xie, M. Zhou and Y. Cui, *Advanced Energy Materials*, 2011, **1**, 523-527.
2. S. W. Lee, B. M. Gallant, H. R. Byon, P. T. Hammond and Y. Shao-Horn, *Energy & Environmental Science*, 2011, **4**, 1972-1985.
3. N. Du, H. Zhang, J. Yu, P. Wu, C. Zhai, Y. Xu, J. Wang and D. Yang, *Chemistry of Materials*, 2009, **21**, 5264-5271.
4. Y. Qi, N. Du, H. Zhang, X. Fan, Y. Yang and D. Yang, *Nanoscale*, 2012, **4**, 991-996.
5. J. Chmiola, C. Largeot, P.-L. Taberna, P. Simon and Y. Gogotsi, *Science*, 2010, **328**, 480-483.
6. Z. Guo, X. Dong, D. Zhou, Y. Du, Y. Wang and Y. Xia, *RSC Advances*, 2013, **3**, 3352-3358.
7. L. Qiu, Z. Shao, W. Wang, F. Wang, D. Wang, Z. Zhou, P. Xiang and C. Xu, *RSC Advances*, 2014, **4**, 24859-24862.
8. Q.-H. Wu, B. Qu, J. Tang, C. Wang, D. Wang, Y. Li and J.-G. Ren, *Electrochimica Acta*, 2015, **156**, 147-153.
9. A. M. Chockla, J. T. Harris, V. A. Akhavan, T. D. Bogart, V. C. Holmberg, C. Steinhagen, C. B. Mullins, K. J. Stevenson and B. A. Korgel, *Journal of the American Chemical Society*, 2011, **133**, 20914-20921.
10. S. Jeong, J.-P. Lee, M. Ko, G. Kim, S. Park and J. Cho, *Nano letters*, 2013, **13**, 3403-3407.
11. C. K. Chan, H. Peng, G. Liu, K. McIlwrath, X. F. Zhang, R. A. Huggins and Y. Cui, *Nature nanotechnology*, 2008, **3**, 31-35.

12. T. Hatchard and J. Dahn, *Journal of The Electrochemical Society*, 2004, **151**, A838-A842.
13. X. Wang, Z. Li, J. Shi and Y. Yu, *Chemical reviews*, 2014, **114**, 9346-9384.
14. S. Jing, H. Jiang, Y. Hu and C. Li, *Nanoscale*, 2014, **6**, 14441-14445.
15. W. Xu and J. C. Flake, *Journal of the Electrochemical Society*, 2010, **157**, A41-A45.
16. W. Wang, M. K. Datta and P. N. Kumta, *Journal of Materials Chemistry*, 2007, **17**, 3229-3237.
17. Z. Wen, J. Yang, B. Wang, K. Wang and Y. Liu, *Electrochemistry Communications*, 2003, **5**, 165-168.
18. X. Xin, X. Zhou, F. Wang, X. Yao, X. Xu, Y. Zhu and Z. Liu, *Journal of Materials Chemistry*, 2012, **22**, 7724-7730.
19. J. K. Lee, K. B. Smith, C. M. Hayner and H. H. Kung, *Chemical Communications*, 2010, **46**, 2025-2027.
20. X. Gao, J. Li, Y. Xie, D. Guan and C. Yuan, *ACS applied materials & interfaces*, 2015, **7**, 7855-7862.
21. Y. Yang, G. Yu, J. J. Cha, H. Wu, M. Vosgueritchian, Y. Yao, Z. Bao and Y. Cui, *Acs Nano*, 2011, **5**, 9187-9193.
22. B. Wang, X. Li, T. Qiu, B. Luo, J. Ning, J. Li, X. Zhang, M. Liang and L. Zhi, *Nano letters*, 2013, **13**, 5578-5584.
23. M. Winter, J. O. Besenhard, M. E. Spahr and P. Novak, *Advanced materials*, 1998, **10**, 725-763.
24. I. Lahiri, S.-W. Oh, J. Y. Hwang, S. Cho, Y.-K. Sun, R. Banerjee and W. Choi, *ACS nano*, 2010, **4**, 3440-3446.
25. X.-M. Liu, Z. dong Huang, S. woon Oh, B. Zhang, P.-C. Ma, M. M. Yuen and J.-K. Kim, *Composites Science and Technology*, 2012, **72**, 121-144.
26. D. Chattopadhyay, I. Galeska and F. Papadimitrakopoulos, *Journal of the American Chemical Society*, 2003, **125**, 3370-3375.
27. B. J. Landi, H. J. Ruf, C. M. Evans, C. D. Cress and R. P. Raffaelle, *The Journal of Physical Chemistry B*, 2005, **109**, 9952-9965.
28. H. Liu, K. Cao, X. Xu, L. Jiao, Y. Wang and H. Yuan, *ACS applied materials & interfaces*, 2015.
29. H. Xiang, K. Zhang, G. Ji, J. Y. Lee, C. Zou, X. Chen and J. Wu, *Carbon*, 2011, **49**, 1787-1796.
30. J. Luo, X. Zhao, J. Wu, H. D. Jang, H. H. Kung and J. Huang, *The Journal of Physical Chemistry Letters*, 2012, **3**, 1824-1829.
31. X. Zhou, A.-M. Cao, L.-J. Wan and Y.-G. Guo, *Nano Research*, 2012, **5**, 845-853.
32. C. Wang, Y.-S. Chui, R. Ma, T. Wong, J.-G. Ren, Q.-H. Wu, X. Chen and W. Zhang, *Journal of Materials Chemistry A*, 2013, **1**, 10092-10098.
33. J.-G. Ren, C. Wang, Q.-H. Wu, X. Liu, Y. Yang, L. He and W. Zhang, *Nanoscale*, 2014, **6**, 3353-3360.
34. F. Yao, F. Güneş, H. Q. Ta, S. M. Lee, S. J. Chae, K. Y. Sheem, C. S. Cojocaru, S. S. Xie and Y. H. Lee, *Journal of the American Chemical Society*, 2012, **134**, 8646-8654.
35. Z. Chen, W. Ren, L. Gao, B. Liu, S. Pei and H.-M. Cheng, *Nature materials*, 2011, **10**, 424-428.
36. H. Sahin, O. Leenaerts, S. Singh and F. Peeters, *arXiv preprint arXiv:1502.05804*, 2015.
37. M. N. Nair, Université de Haute Alsace-Mulhouse, 2013.
38. C. Wang, Y. Li, Y.-S. Chui, Q.-H. Wu, X. Chen and W. Zhang, *Nanoscale*, 2013, **5**, 10599-10604.
39. C. Peng, H. Chen, Q. Li, W. Cai, Q. Yao, Q. Wu, J. Yang and Y. Yang, *Journal of Materials Chemistry A*, 2014, **2**, 13859-13867.
40. T. Mondal, A. K. Bhowmick and R. Krishnamoorti, *Journal of Materials Chemistry*, 2012, **22**, 22481-22487.
41. M. Holzapfel, H. Buqa, L. J. Hardwick, M. Hahn, A. Würsig, W. Scheifele, P. Novák, R. Kötz, C. Veit and F.-M. Petrat, *Electrochimica acta*, 2006, **52**, 973-978.
42. X. Zhou, Y.-X. Yin, L.-J. Wan and Y.-G. Guo, *Chemical Communications*, 2012, **48**, 2198-2200.
43. B. Li, F. Yao, J. J. Bae, J. Chang, M. R. Zamfir, D. T. Le, D. T. Pham, H. Yue and Y. H. Lee, *Scientific reports*, 2015, **5**.
44. J. G. Ren, Q. H. Wu, G. Hong, W. J. Zhang, H. Wu, K. Amine, J. Yang and S. T. Lee, *Energy Technology*, 2013, **1**, 77-84.
45. A. Ghosh and Y. H. Lee, *ChemSusChem*, 2012, **5**, 480-499.
46. X. Li, J. H. Cho, N. Li, Y. Zhang, D. Williams, S. A. Dayeh and S. Picraux, *Advanced Energy Materials*, 2012, **2**, 87-93.
47. H. Y. Yue, S. Huang, J. Chang, C. Heo, F. Yao, S. Adhikari, F. Gunes, L. C. Liu, T. H. Lee and E. S. Oh, *ACS nano*, 2014, **8**, 1639-1646.

Figure 1

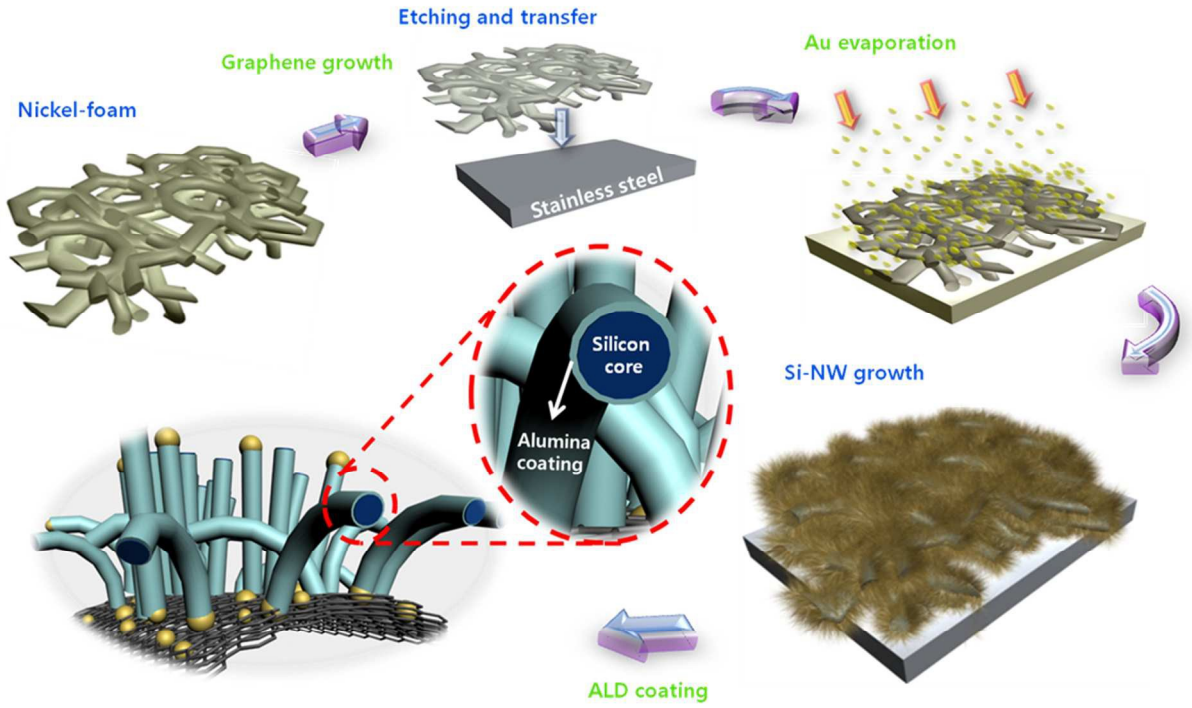

[a] **Figure 1.** Schematic illustration of graphene foam synthesis, transfer, e-beam evaporation of Au catalyst, Si nanowire (SiNWs) growth and atomic layer deposition of alumina (ALD).

Figure 2

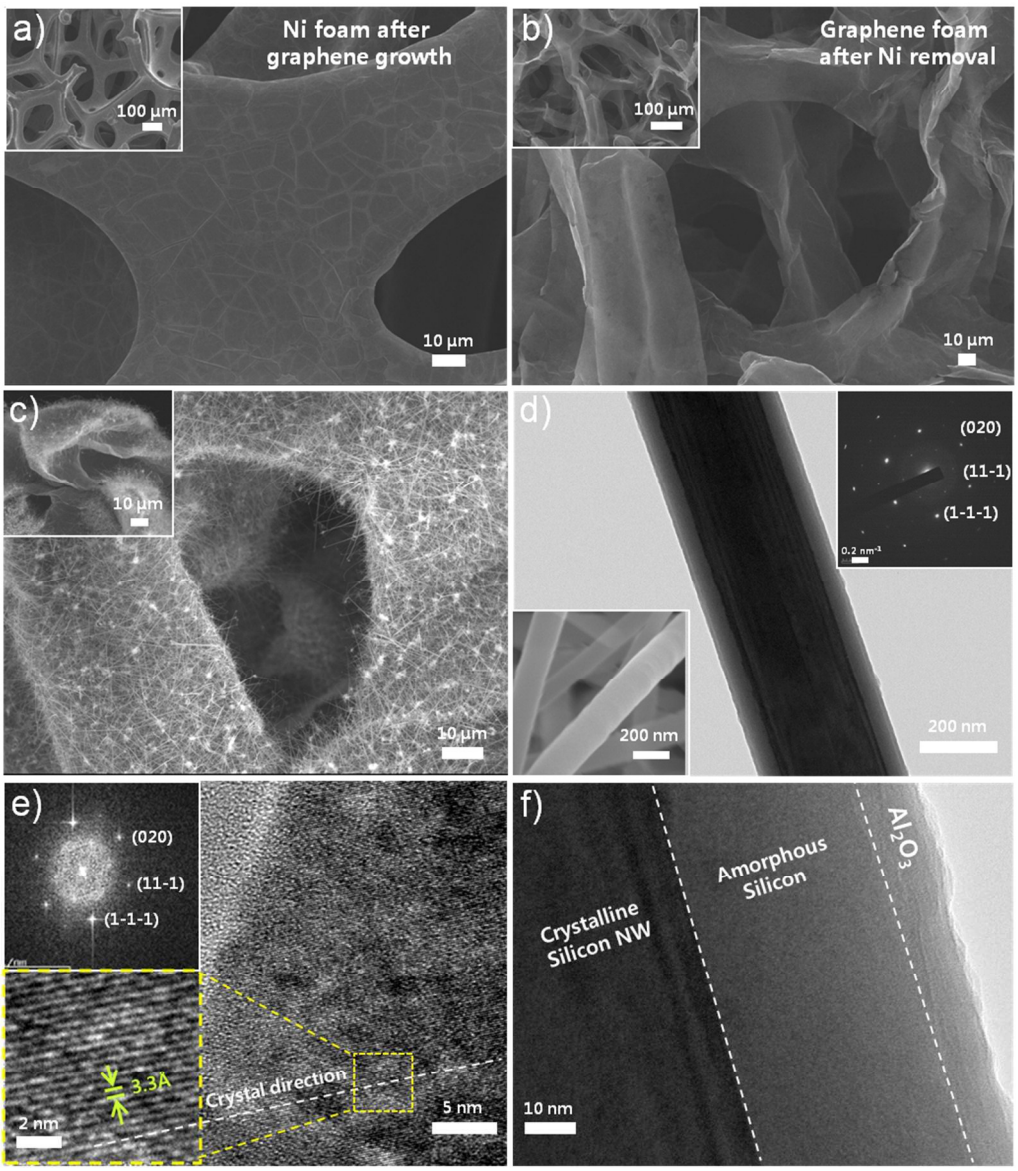

b. **Figure 2.** Morphologies of graphene foam and Si-nanowires (SiNWs); SEM images of (a) graphene on Ni foam, and (b) graphene foam after Ni removal. Insets: low magnification SEM images. (c) SEM images after SiNWs growth. Inset: cross-section view from GF/SiNWs composite. (d) TEM image of an individual SiNW after alumina coating (ALD). Insets: (Top) SAED pattern of SiNWs and (Bottom) magnified SEM image from SiNWs. (e) High magnification images of TEM showing crystal formation of core SiNWs. Inset: (Top) FFT calculated crystal pattern of core SiNW and (Bottom) magnified crystallographic image from dotted square. (f) HR-TEM image from an individual SiNW showing crystalline core, amorphous Si-shell and ALD of 10 nm alumina layer.

Figure 3

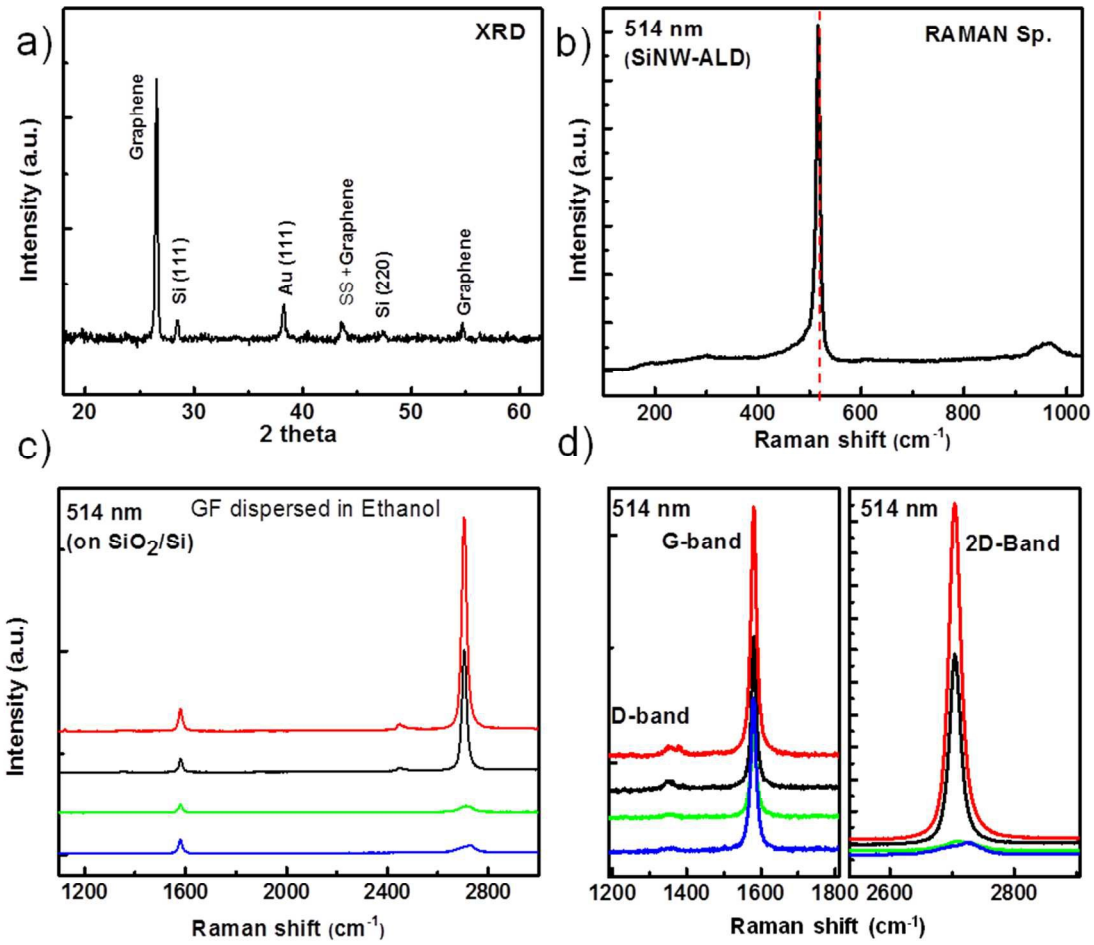

Figure 3 a) XRD patterns from as-prepared GF/SiNWs composite showing graphene peaks and crystalline Si peaks. Raman spectroscopy of (b) alumina-coated (ALD) SiNWs showing a sharp peak at ~520 cm^{-1} (c) graphene foam dispersed in ethanol solution and spin-coated on Si/SiO_2 substrate with various number of layers, from monolayer up to multiple layers showing the quality of graphene with very small D- peaks. (d) magnified D-band, G-band and 2D-band spectra from the same plot of Raman spectrum in (c).

Figure 4

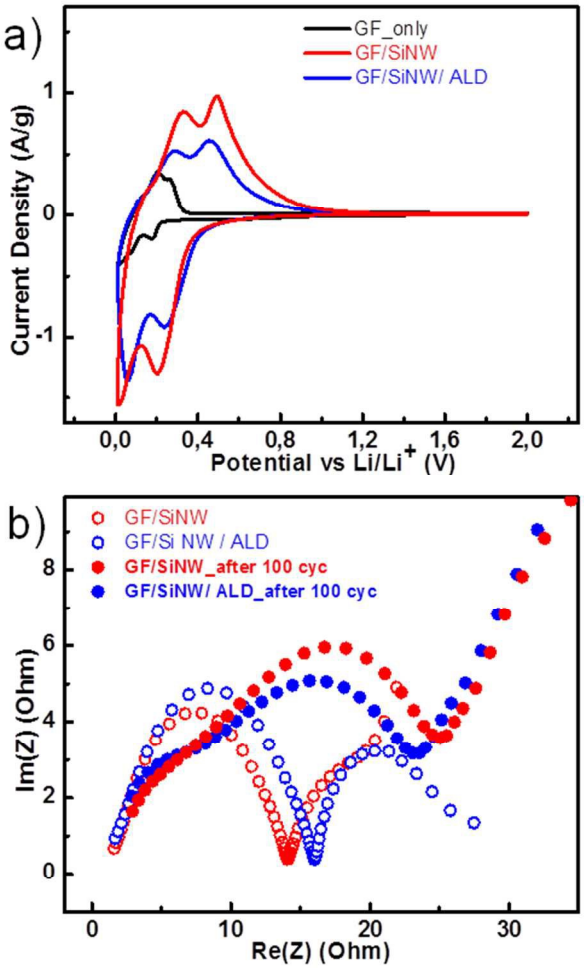

Figure 4 (a) Cyclic voltammetry profiles (2nd cycle) of GF-only (black), GF/SiNWs composite with (blue) and without alumina coating (ALD) (red) at a scan rate of 0.1 mVs^{-1} in the voltage range of 0.01-2 V. (b) Nyquist plots of GF/SiNWs composite with (red circles) and without ALD (black circles), as prepared (hollow circles) and after 100 discharge/charge cycles (solid circles) by applying a sine wave with an amplitude of 20 mV over a frequency range of 100 kHz to 10 mHz.

Figure 5

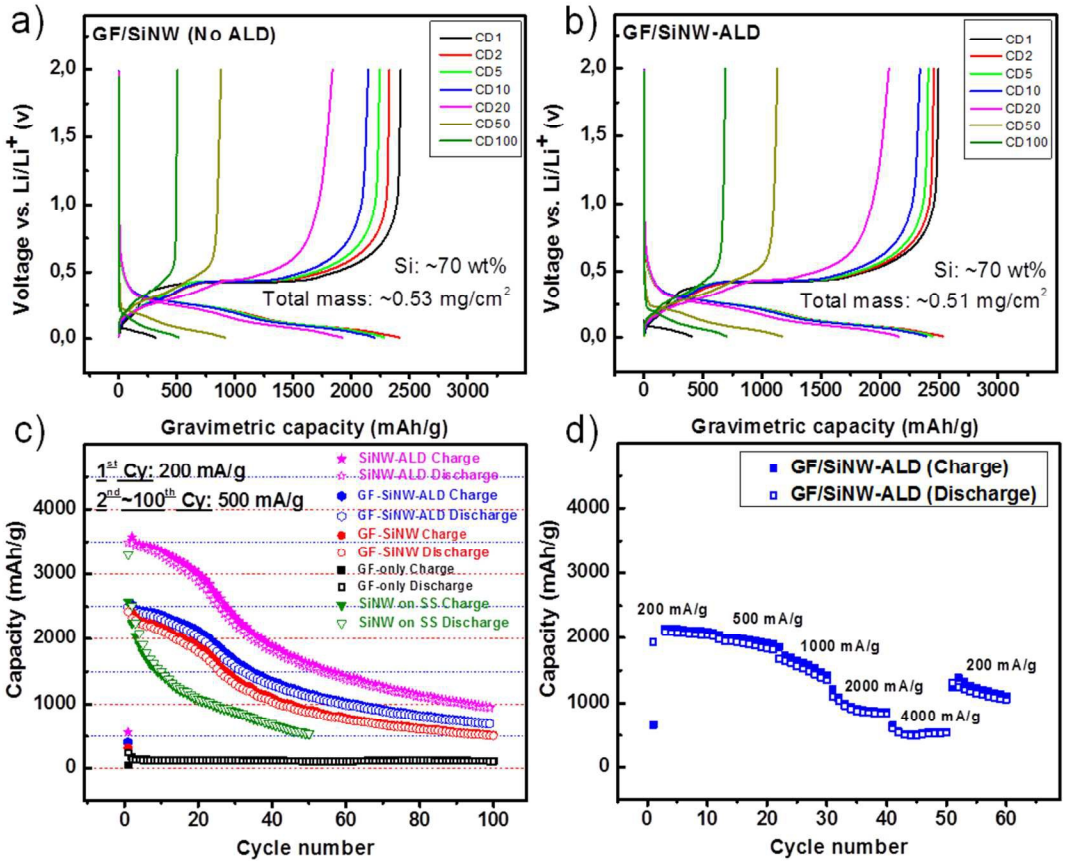

Figure 5. Voltage profiles of GF/SiNWs composite for the first, second, fifth, tenth, twentieth and Fiftieth cycles for (a) as-prepared, and (b) alumina-coated (ALD) samples c) Comparison of capacity cycling profiles for GF-only (Black square) , pure SiNWs on stainless-steel (SS) (green triangular), GF/SiNWs composite without ALD (red circle) and GF/SiNWs composite with ALD (blue hexagon based on Si mass only, cycled at a constant current of 200 mA.g^{-1} in the first and 500 mA.g^{-1} in the remaining charge (solid)/ discharge(hollow) cycles. (d) Rate capability of GF/SiNWs composite with currents of 200, 500, 1000, 2000 and 4000 mA.g^{-1} for 10 cycles at each current.

Figure 6

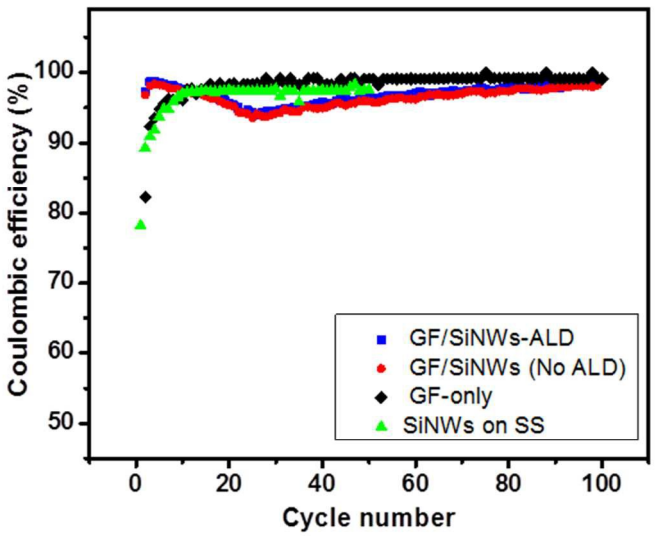

Figure 6. Coulombic efficiency profile for SiNWS on stainless steel (SS) (green triangular), GF_only (Black diamond), as prepared GF/SiNWs composite (red circle) and GF/SiNWs composite with alumina coating (ALD) (blue square).

Figure 7

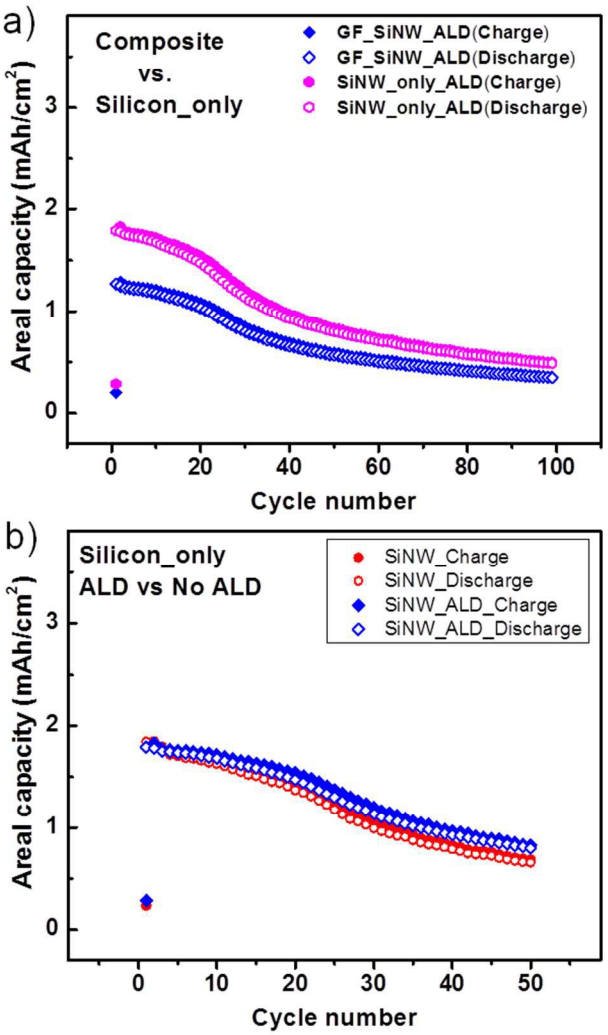

Figure 7. (a) Comparison of the areal capacities of the alumina coated (ALD) GF/SiNW composite with total mass (blue) and with only SiNW mass (magenta) cycled at a constant current of 200 mA.g^{-1} in the first and 500 mA.g^{-1} in the remaining charge (solid)/ discharge (hollow) cycles. (b) Areal capacities comparison of as-prepared SiNWs (red) and alumina coated (ALD) SiNWs (blue) at a constant current of 200 mA.g^{-1} in the first and 500 mA.g^{-1} in the remaining charge (solid)/ discharge(hollow) cycles. Potential window for all measurements are between 0.01V and 2V.

Figure 8

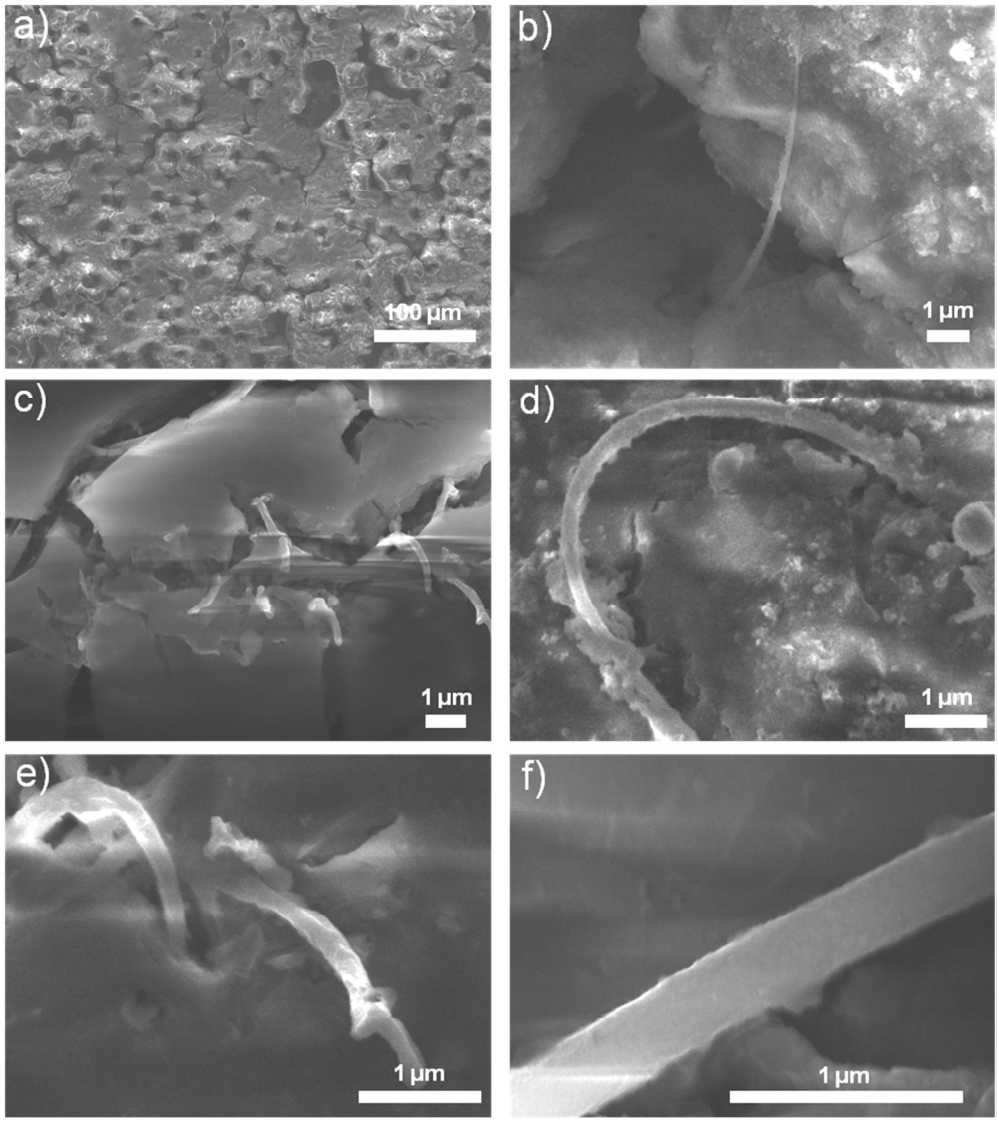

Figure 8. SEM images after 100 cycles from the alumina-coated (ALD) GF/SiNWs composites

Graphical Abstract

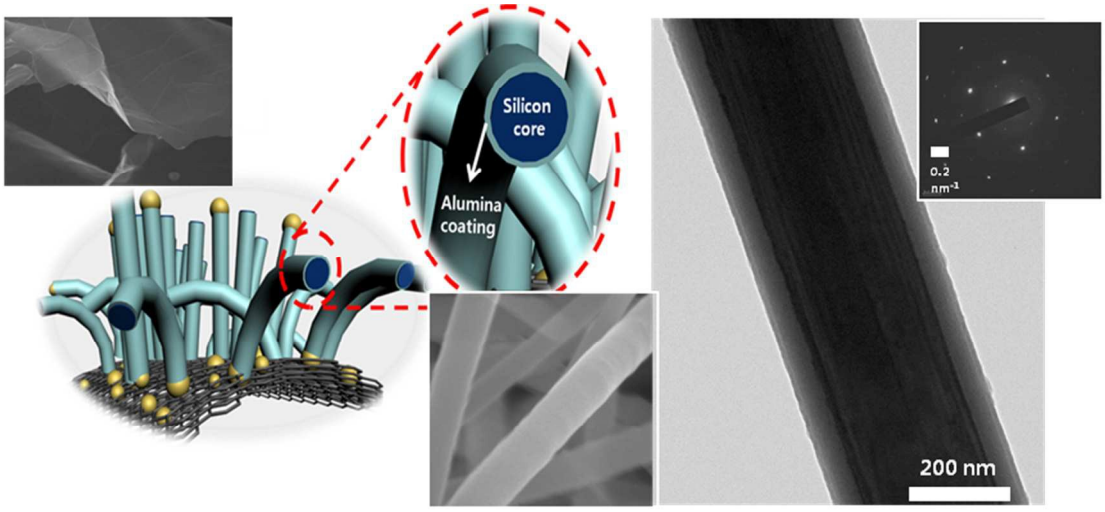

A facile direct fabrication route to synthesis of Si-nanowires on a highly conductive porous 3D graphene network of graphene foams, with improved Si-mass loadings is demonstrated. Graphene foams underneath the Si-nanowires utilized as a conductive and a flexible support to enhance the gravimetric and areal capacities at reasonable current densities. Graphene foams' excellent elastic property improved the stress induced pulverization of Si-nanowires, resulting in a better cycling performance of the final composite. ALD coating of composite further improved the cycle life.